PNAS
www.pnas.org

Supplementary Information for

Structural basis for the activation of the DEAD-box RNA helicase DbpA by the nascent ribosome

Jan Philip Wurm*, Katarzyna-Anna Glowacz, Remco Sprangers*

Institute of Biophysics and Physical Biochemistry, Regensburg Center for Biochemistry, University of Regensburg, 93053 Regensburg, Germany.

*Corresponding Authors:
E-mail: remco.sprangers@ur.de
E-mail: jan-philip.wurm@ur.de

This PDF file includes:

SI Materials and Methods.

Protein expression and purification

The gene coding for full length DbpA and two fragments that comprise the N-terminal RecA domain (residues 1-214) or the C-terminal RecA domain plus the RRM (residues 209-457) were PCR amplified from genomic *E. coli* DNA (strain BL21(DE)) and cloned into a modified pETM11 vector that contains a tobacco etch virus (TEV)-protease cleavable, N-terminal hexahistidine tag. Point mutations were introduced by site directed mutagenesis following the QuickChange approach. For a list of DbpA constructs used in this study see **SI Appendix, Table S2**.

For protein expression the plasmids were transformed into *E. coli* BL21(DE) cells. Cells were grown in M9 medium (H_2O based for protonated samples or D_2O based for deuterated samples) containing 0.5 g/l $^{15}NH_4Cl$ and 2 g/l (deuterated) glucose. In order to adapt the cells to D_2O-M9 medium the cells from an initial preculture in LB medium were transferred to 10 % of the final volume of D_2O-M9 medium to an OD_{600} of 0.15 and grown over night at 37 °C. This culture was used to inoculate the remaining D_2O-M9 medium. Cells were grown to an OD_{600} of 0.7-0.9 at 37 °C, then IPTG was added to a concentration of 1 mM and proteins were expressed at 25 °C over night. For $^{1}H,^{13}C$ labeling of the methyl groups of Ile (Cδ methyl only), Val, Leu, Met and Ala (ILMVA) in a $^{2}H,^{15}N$ labeled background 60 mg/l 2-Ketobutyric acid-(4-^{13}C,3,3-d2), 100 mg/l 2-Keto-3-methyl-butyric acid-(dimethyl-$^{13}C_2$, 3-d), 100 mg/l L-methionine-(methyl-^{13}C) and 100 mg/l L-alanine-(methyl-^{13}C, 2-d) were added to the medium. For additional $^{1}H^{13}C$ labeling of the Thr methyl groups the DLAM-$I^{\delta1}$-T^{γ} kit (NMR-BIO, Grenoble, France) was used (the Ile precursor 2-Ketobutyric acid-(4-^{13}C,3,3-d2) was omitted in this case). Selective protonation of the Tyr aromatic and Hβ positions was achieved by addition of 150 mg/l 4-hydroxyphenylpyruvic acid (1, 2). All precursors were added 1 h prior to induction except for alanine, which was added 20 min before induction.

After expression cells were harvested by centrifugation, resuspended in buffer A (400 mM NaCl, 50 mM sodium phosphate, pH 7.4, 10 mM imidazole) supplemented with 0.1 % (v/v) triton x-100 and 1 mg/ml lysozyme and lysed by sonication. Cell debris was removed by centrifugation and the supernatant was loaded onto a gravity flow Ni-NTA column equilibrated in buffer A. The column was washed with wash buffer (1 M NaCl, 25 mM sodium phosphate, pH 7.4) to remove nucleic acids bound to DbpA and with buffer A supplemented with 20 mM imidazole. DbpA was eluted with elution buffer (150 mM NaCl, 25 mM sodium phosphate, pH 7.4, 300 mM imidazole). The hexahistidine tag was removed by TEV protease cleavage during dialysis over night at 4 °C against dialysis buffer (150 mM NaCl, 25 mM sodium phosphate, pH 7.4, 1 mM DTT). DbpA was loaded onto a NiNTA column equilibrated in dialysis buffer. The flowthrough was collected, mixed with ½ vol-

ume of 60 % glycerol (v/v) and loaded onto a 5 ml HiTrap HP heparin column. DbpA was eluted using a 10 % - 50 % gradient over 50 ml (buffer A: 25 mM HEPES, pH 7.3, 20 % (v/v) glycerol, buffer B: as buffer A + 1 M NaCl). As the final purification step DbpA was subjected to size exclusion chromatography (SEC) using a Superdex 75 16/600 column (SEC buffer: 125 mM NaCl, 25 mM HEPES, pH 7.3, 1 mM DTT). NMR samples were prepared in SEC buffer supplemented with 5 % (v/v) D_2O.

Structure determination of the RecA_C/RRM construct

Two samples with different labeling schemes were used for the structure determination of the RecA_C/RRM construct. The initial sample was protonated and ^{13}C labeled at the methyl groups of Ile (Cδ methyl only), Leu, Met, Val and Ala (ILMVA labeling scheme) in a $^{2}H,^{15}N$ labeled background. Preliminary structures indicated that a large part of the interface between the RecA_C and RRM domains was formed by Y426 and T385 on the RRM side. Subsequently, a second sample was prepared where in addition to the ILMVA labeling scheme the Thr methyl group was protonated and ^{13}C labeled and the Tyr aromatic and Hβ positions were protonated in a $^{2}H,^{15}N$ labeled background (ILMVATY labeling scheme). Both samples had a protein concentration of 800 µM. To increase the solubility and long term stability of the samples the NaCl concentration was increased to 250 mM and 25 mM Arg/Glu was added to the sample buffer.

The assignment of the backbone amide and ILMVA methyl groups of the RecA_C/RRM construct was published previously (3). These assignments were expanded to the Thr methyl groups and the aromatic protons of the two Tyr residues using 3D-HCH-, 3D-CCH- and 3D-HNH-NOESY spectra. The 3D-HCH-NOESY spectrum was recorded in D_2O based buffer to facilitate the assignment of the aromatic protons. Stereospecific methyl group assignment for 21 out of 46 Leu and Val residues could be obtained by preparing a protonated sample with 10 % fractional ^{13}C labeling as described by Neri et al. (4). In addition 11 out of 26 Ser and Thr hydroxyl groups were assigned based on 3D-HCH- and 3D-HNH-NOESY spectra.

For the structure calculations a combination of manual NOE assignment and the automated NOE assignment protocol implemented in CYANA 3.98 was used (5). Distance restraints were based on the following NOESY experiments: 3D-HNH- and 3D-CNH-NOESY spectra recorded on the ILMVA labeled sample and on 3D-HNH-, 3D-CCH-, 3D-HCH-NOESY spectra recorded on the ILMVATY labeled sample. All spectra were recorded with NOE mixing times of 250 ms using SOFAST-HMQC based pulse sequences (6) for the methyl proton detected experiments and HSQC based pulse sequences for the amide proton detected experiments. Except for the 3D-CNH-NOESY spectrum where the carbon evolution was of the HMQC type and the nitrogen evolution of the

HSQC type (7). The peaks were picked using the 3D peak picking algorithm of NMR-FAM SPARKY 1.414 (8) and then manually corrected to remove falsely picked artifacts. In total the final peaklists contained 9009 NOE peaks of which 7795 (86 %) were assigned (676 (8 %) manually and 7119 (79 %) by automated NOE assignment). In addition to the NOE based upper distance restraints backbone dihedral angle restraints for 207 residues were included in the calculations. These restraints were derived from backbone H, N, CO, Cα and Cβ chemical shifts using TALOS-N (9).

In the final structure calculation 58 backbone hydrogen bond restraints were added, which were derived as follows: A sample of $^{2}H^{15}N$ labeled RecA_C/RRM in NMR buffer was lyophilized, dissolved in the same volume of D_2O and subsequently a ^{15}N-TROSY spectrum was recorded. Backbone amides whose signals were detectable in this spectrum were assumed to be protected by stable hydrogen bonds. Hydrogen bond restraints were introduced for those residues, which showed hydrogen bonds in at least 10 of the 20 best structures in the previous calculation performed without hydrogen bond restraints.

In the final round 100 structures were calculated and the 20 structures with the lowest target function were chosen to represent the solution structure ensemble. A representative mean structure was calculated as described by Gottstein et al. (10) and included as the first model in the final pdb file (the structure with the highest target function was discarded to keep the number of models constant).

Structures were analyzed and structure figures were generated with UCSF ChimeraX (11).

Additional NMR measurements

$\{^{1}H\}$-^{15}N hetNOE values were recorded at 800 MHz using the TROSY based pulse sequence from Lakomek et al. (12) and a saturation time of 8 s preceded by a recycling delay of 1 s.

NMR titration experiments were performed in SEC buffer using the following concentrations: DbpA 60 µM, RNA 75 µM, ADPNP 2 mM, ATP 4 mM (ADPNP/ATP were added together with 5 mM $MgCl_2$). CSPs were calculated according to

$CSP = ((\Delta C/4)\text{^}2+(\Delta H)\text{^}2))^{0.5}$

(with ΔC, ΔH chemical shift difference in ppm in the ^{13}C and ^{1}H dimensions). Due to the size of full length DbpA and the magnitude of the CSPs, we could not obtain a full resonance assignment of the closed state. For the closed state (**Fig. 2b**) we thus report only the minimal CSPs (13) and the real CSPs could be larger than the reported values.

The ILMVA methyl group assignments of the free RecA_C/RRM construct were transferred to the (N_{14})HP92 bound state using SOFAST-HMQC based 3D-CCH- and 3D-HCH-NOESY spectra (mixing time 250 ms). The sample contained 300 µM ILMVATY labeled RecA_C/RRM construct and

450 µM (N_{14})HP92 RNA in 25 mM HEPES, pH 7.3, 180 mM NaCl, 1 mM DTT, 5 % D_2O. The same spectra were used for the detection of the interdomain NOE crosspeaks between V285 in the RecA_C domain and A419 in the RRM.

The sample for the detection of the NOE crosspeak between M114 in the RecA_N domain and A423 in the RRM contained 250 µM ILMVA labeled full length DbpA, 350 µM (N_{14})HP92 RNA, 110 mM NaCl, 25 mM Arg/Glu, 25 mM HEPES, pH 7.3, 1 mM DTT, 5 mM $MgCl_2$, 2 mM ADP, 4 mM BeF_2 and 15 mM NaF. The ATP analog ADP/BeF_3 was used instead of ADPNP to ensure sample stability during the long term NOE experiments (SOFAST-HMQC based 3D-CCH- and 3D-HCH-NOESY spectra with a mixing time of 250 ms). The same closed state is formed in the presence of ADP/BeF_3 or ADPNP (**SI Appendix, Fig. S15**) as the methyl TROSY spectra are virtually identical.

^{1}H-^{15}N correlation spectra of the GU-^{15}N labeled (N_{14})HP92 RNA were recorded using SOFAST-HMQC experiments at an RNA concentration of 100 µM in SEC buffer supplemented with 5 % (v/v) D_2O and 5 mM $MgCl_2$. 130 µM DbpA and 2 mM ADPNP were added to form the DbpA/RNA complex and the closed conformation. The imino proton signals of the RNA stem were assigned using ^{1}H-NOESY experiments conducted at 277 K.

NMR spectra were recorded at 298 K on 600 and 800 MHz Bruker Neo Avance NMR spectrometers equipped with nitrogen (600 MHz) or helium cooled (800 MHz) cryoprobes. Spectra were processed with Topspin 4.0.2 or NMRPipe 9.6 (14) and analyzed using NMR-FAM SPARKY 1.414 (8) and CARA 1.9.1.7 (15).

ATPase assays

The ATPase activity of DbpA was determined using a coupled pyruvate kinase-lactate dehydrogenase assay as described previously (16). The assay couples regeneration of ATP from ADP to the oxidation of NADH, which can be followed by UV-absorption at 340 nm. The assay was adapted to 96-well plate format (17) and performed using a TECAN spark plate reader at 25 ºC. The reactions (total volume 150 µl) consisted of 3 mM ATP, 5 mM $MgCl_2$, 0.5-2 µM DbpA, 450 µM NADH, 1.5 mM pyruvate, 5 u/ml pyruvate kinase/lactate dehydrogenase (from rabbit muscle, Sigma Aldrich, #P0294), 5 µM RNA (except for N_{32} RNA which was used at 50 µM to ensure saturation of DbpA) in SEC buffer. Absorption measurements at 340 nm were performed every 20 s for 2-4 h. Catalytic rates (k_{obs}) were determined based on the slope of the absorbance decline (dA_{340}/dt) in the linear region of the time course based on the following equation (17):

$$k_{obs} = - dA_{340}/dt*(1/K_{path})*(1/[DbpA])$$

, where [DbpA] is the DpbA concentration and K_{path} is the molar absorption coefficient of NADH at 340 nm for the path length in the 96-well plate (2.22 1/mM). K_{path} was calibrated using NADH solution of known concentration. Rates were corrected for background ATP hydrolysis and NADH decomposition using control reaction lacking DbpA. The reported values are average and standard deviation of 3 independent measurements.

RNA production and purification

RNAs were prepared by *in vitro* transcription (IVTC) using T7 RNA polymerase (P266L mutant (18), produced in-house). DNA oligonucleotides that are double stranded in the T7 promotor region (19) were used as templates, except for the H90_5' and H90_3' RNAs, where PCR products were used as templates. IVTCs consisting of 40 mM Tris/HCl, pH 8.0, 0.01 % (v/v) Triton X-100, 20-40 mM $MgCl_2$, 1 mM spermidine, 5 mM DTT, 4 mM of each NTP, 40 µg/ml T7 polymerase, 1 µM DNA template were incubated at 37 °C for 3 h. For ^{15}N labelling of the (N_{14})HP92 RNA ^{15}N-labeled GTP and UTP were used for IVTC. After IVTC 50 mM EDTA, pH 8.0 was added and the RNA was precipitated by addition of 1 volume of isopropanol. After centrifugation the RNA pellet was dissolved in H_2O and the RNA was purified by denaturing anion exchange HPLC on a 22 × 250 mm DNAPac PA100 column (Dionex) operated at 80°C (buffer A: 5 M Urea, 20 mM Tris/HCl, pH 8.0 (adjusted at room temperature), buffer B: as A + 2 M NaCl). The RNAs were eluted using a linear gradient from buffer A to B that was optimized for each RNA. Fractions containing the RNA of interest were identified by denaturing urea polyacrylamide gel electrophoresis (PAGE), pooled and precipitated with 1 volume of isopropanol (for short RNAs < ~20 nt 300 mM NaCl was added to facilitate the precipitation). After centrifugation the RNA pellet was washed with 70 % (v/v) ice cold ethanol, air dried and resuspended H_2O. RNAs were folded by heating to 95 °C for 1 min followed by rapid cooling on ice. Homogeneous folding of the RNAs was checked by native PAGE.

5' fluorescein labeled and unlabeled 9mer RNAs (N_9 and $N_{9'}$) for helicase assays were commercially obtained from Integrated DNA Technologies (Coralville, USA).

See **SI Appendix, Table S3** for RNA sequences.

Modeling of the closed state of DbpA

The model of the DbpA closed conformation was constructed using UCSF chimera (20): First the closed conformation of the DbpA RecA domains (residues 1-365) was modeled based on the closed conformation of the DEAD box helicase Vasa (PDB ID 4d25)(21) using the SWISS model server (22). On this model the NMR structure with the lowest target function was superimposed based on the RecA_C domains. Finally the Vasa based model of the RecA_C domain was removed. The rela-

tive orientation of the RecA domains in the model is thus based on the Vasa structure, whereas the relative orientation of the RRM and core domains is based on the NMR structure.

To model the closed state in complex with 31mer RNA (**Fig. 4a**) the structure of the YxiN RRM in complex with the 23S rRNA (PDB ID 3moj) (23) was superimposed on the DbpA RRM. Then all nucleotides except the 15 nt of HP92 (nt 2547-2561) (shown in violet in **Fig. 4a**) and the Yxin RRM were removed. The 5 nt bound to the ssRNA binding site of the helicase core were modeled by superimposing the Vasa structure (PDB ID 4d25) on the DbpA core domains and removing all residues except for the RNA. The final model is thus composed of the RecA_N domain based on the Vasa helicase, the RecA_C and RRM domains from our NMR structure, HP92 from the YxiN structure and the nucleotides bound to the core from the Vasa structure. Finally nt 1-2, 8-14, 30-31 of the RNA (shown in pink in **Fig. 4a**) that are not bound by the RRM or the helicase core were modeled in CYANA (5) by fixing all other residues and executing the regularize script.

The model of DbpA in complex with the 23S rRNA (nt 2508-2581) (**Fig. 5a**) was modeled by superimposing the YxiN RRM in complex with the 23S rRNA on the DbpA RRM and then removing the YxiN RRM. Some clashes are observed between the 5' part of H90 and the RecA_N domain in this model, but, based on the following observations, this region of the RNA is most likely flexible in solution: The 5' part of H90 does not directly interact with the RRM, its orientation is mainly stabilized by crystal packing contacts and it is connected to the 3' part of H90 by a flexible bulge that is not visible in the crystal structure (nt 2572-2576).

PRE-measurements

The (N_{12})HP92 RNA for the PRE-measurements was obtained commercially from Dharmacon (Lafayette, USA). The (N_{12})HP92 RNA contains a 4-Thiouridine at the 5' end which was labeled with 4-(2-Iodoacetamido)-TEMPO by incubating the RNA at a concentration of 120 uM at room temperature for 24 h in the dark in a solution containing 100 mM HEPES, pH 8.0, 10 mM 4-(2-Iodoacetamido)-TEMPO and 20 %(v/v) DMSO. Free label was removed by two sodium acetate/ EtOH precipitation steps. PRE measurements were performed in SEC buffer without DDT using the following concentrations: DbpA 55 µM, TEMPO-labeled (N_{12})HP92 RNA 72 µM, ADPNP 2 mM, $MgCl_2$ 5 mM. SOFAST-HMQC spectra were recorded before and after reduction of the TEMPO spin label by addition of 2 mM sodium ascorbate. Peaks were integrated using NMRPipe (14). PRE values were calculated as the ratio I_{SL}/I_0, where I_{SL} and I_0 are the peak integrals in the spectra recorded before and after reduction of the spin label. The following methyl group signals (mainly in the RecA_C and RRM domains) show only small CSP upon formation of the closed conformation and could be readily assigned by comparison of their CCH-NOESY strips: M26, L133, V151, I229,

L232, V257, V264, V269, V285, V314, I355, 3M59, L364, A376, A383, M395, I408, I418, A423, V433. As M161 from the RecA_N domain is placed in closed proximity to the spin label in our model of the closed state we also assigned its methyl group signal by mutation to Ile (see suppl. Fig. S9)

Helicase assays

Unwinding assays were performed in 125 mM NaCl, 25 mM Na/HEPES, pH 7.3, 5 mM $MgCl_2$, 2 mM ATP at 30 °C. Fluorescently labeled 9mer RNAs containing a 5' fluorescein were purchased from IDT. The fluorescently labeled RNAs were annealed to the complementary unlabeled RNA at a concentration of 1 µM labeled to 1.5 µM unlabeled RNA in assay buffer without ATP and DbpA. To this end the RNAs were heated to 95 °C for 1 min and then placed at room temperature for 15 min. Final RNA concentrations were 100 nM labeled 9mer RNA, 150 nM complementary unlabeled RNA and 2 µM unlabeled 9mer RNA with the same sequence as the labeled RNA which prevents reannealing of the labeled 9mer RNA. The DbpA concentration was 2 µM. 20 µl samples were taken after the indicated time points and mixed with 6 µl loading buffer (25 mM EDTA, pH 8.0, 0.5 % (v/v) SDS, 72 % (v/v) glycerol) to stop the reaction. Free RNA was separated from the duplex RNA by native PAGE at 4 °C. Gels were analyzed by fluorescence imaging.

RNA binding measurements by fluorescence anisotropy

(N_{14})HP92, (N_2)HP92 and H90_5' RNAs were labeled with fluorescein-5-thiosemicarbazide (Cayman Chemical) at the 3' end according to Zearfoss and Ryder (24) as follows: 1.5 mM $NaIO_4$ was added to 50 uM RNA in 300 mM NaAcO, pH 5.3 to oxidize the 3' diol to dialdehyde. The solution was incubated at room temperature for 10 min. 2 mM glycerol was added to quench unreacted $NaIO_4$ and the RNA was precipitated with 3 vol. of ethanol. After centrifugation the pellet was re-suspended in 1 volume of 300 mM NaAcO, pH 5.3 and 2.5 mM fluorescein-5-thiosemicarbazide was added from a 100 mM stock solution in DMSO. The reaction mixture was incubated over night at 4 ºC. Finally the RNA was precipitated twice with NaAcO and ethanol to remove free label.

Fluorescence anisotropy measurements were performed at 25 ºC in SEC buffer supplemented with 0.002 % Triton X-100. Fluorescently labeled RNAs were used at 25 nM concentration and solutions with increasing DbpA concentrations were prepared independently. Fluorescence anisotropy was measured using a Tecan spark plate reader, excitation and emission wavelength were set to 485 nm and 535 nm, respectively. Binding curves were fitted to the standard equation for a one-site binding model using in house written Matlab scripts:

$$A = A_0+\Delta A*(([R]+[D]+K_D)/2 - (([R]/2+[D]/2+K_D/2)^2 - [D]*[R])^{0.5})$$

where with A is the anisotropy, A_0 is the anisotropy of free RNA, ΔA is the increase in anisotropy due to binding, [R] is the concentration of fluorescently labeled RNA, [D] is the DbpA concentration and K_D is the dissciation constant of the DbpA/RNA complex. The reported values are average and standard deviation of 3 independent measurements.

Determination of the dissociation rate of the DbpA/H90_5' RNA complex

Dissociation of the DbpA/H90_5' RNA complex was followed by fluorescence anisotropy measurements. To this end the complex between DbpA (-wt or -R331A mutant) and 3' fluorescein labeled H90_5' RNA was formed by incubating 50 nM RNA with 100 nM DbpA in SEC buffer supplemented with 2 mM $MgCl_2$ for 10 min. Then 2 mM ATP was added for measurements in the presence of ATP and baseline fluorescence anisotropy was recorded every 6 s as described above for the RNA binding measurements. After 5 min a 100 fold excess of unlabeled H90_5' RNA (5 µM) was added to prevent rebinding of fluorescently labeled H90_5' RNA. This timepoint was set to 0 in the time traces and dissociation was followed by the decline in fluorescence anisotropy. The dead time of the experiment between addition of RNA and the start of the measurement is approximately 10 s.

Sequence alignments

The sequences of the DEAD box helicases Dbpa and SrmB from *E. coli* were blasted against the UniRef90 database (25)**.** The top 250 sequences were aligned using Clustal Omega (26). Finally all sequences that did not contain all three domains of DbpA were removed from the alignment. The sequence logos were generated using the WebLogo webserver (27).

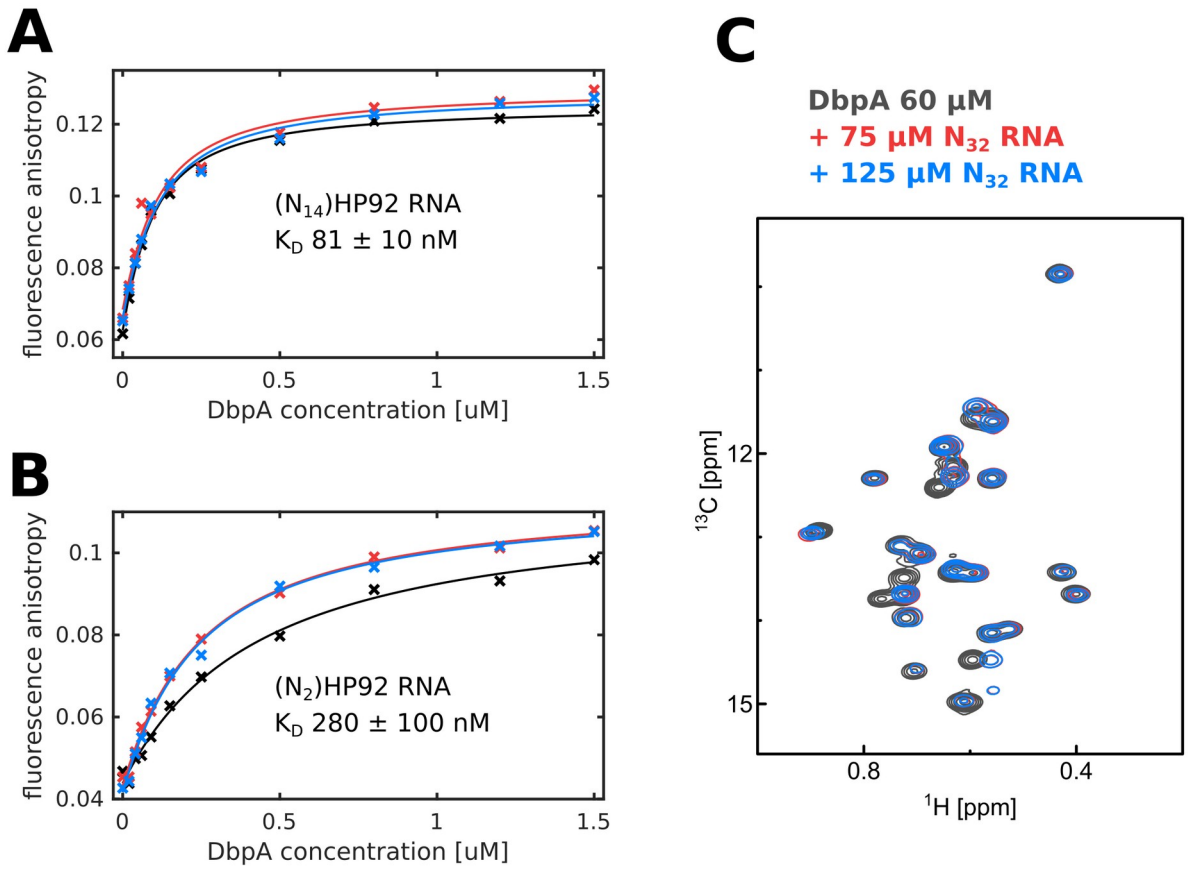

Fig. S1: Concentrations of (N_2)HP92, (N_{14})HP92 and N_{32} RNAs used in NMR titrations and ATPase assays are saturating

(A, B) Titrations of 3' fluorescein labeled (N_{14})HP92 (A) and (N_2)HP92 (B) RNAs with DbpA-wt. Binding is followed by fluorescence anisotropy measurements. Titrations were performed in triplicate (n=3) and are shown in black, red and blue. The dissociation constants were obtained by non-linear fitting (continues lines). Mean and standard deviation of the three dissociation constants are given. The result for the (N_{14})HP92 RNA is in reasonable agreement with the previously reported dissociation constant (9 nM) for a similar construct determined by electrophoretic mobility shift assays (28).

(C) In agreement with previous reports (28) we also observed formation of higher order complexes at µM DbpA concentrations as reflected by a linear increase of the fluorescence anisotropy. This prevented the determination of the k_D between DbpA and the N_{32} RNA by fluorescence anisotropy measurements. We thus resorted to NMR titration of DbpA with N_{32} RNA to show that DbpA is saturated with RNA at the concentrations used in the NMR experiments (75 µM). Methyl-TROSY spectra (Ile region) of 60 µM ILMVA-labeled DbpA-wt are shown for the apo state (black), in the presence of 75 µM (red) and 125 µM (blue) N_{32} RNA. The blue and red spectra are virtually identical, which implies that DbpA is saturated at an N_{32} RNA concentration of 75 µM indicating a k_D in the lower µM range.

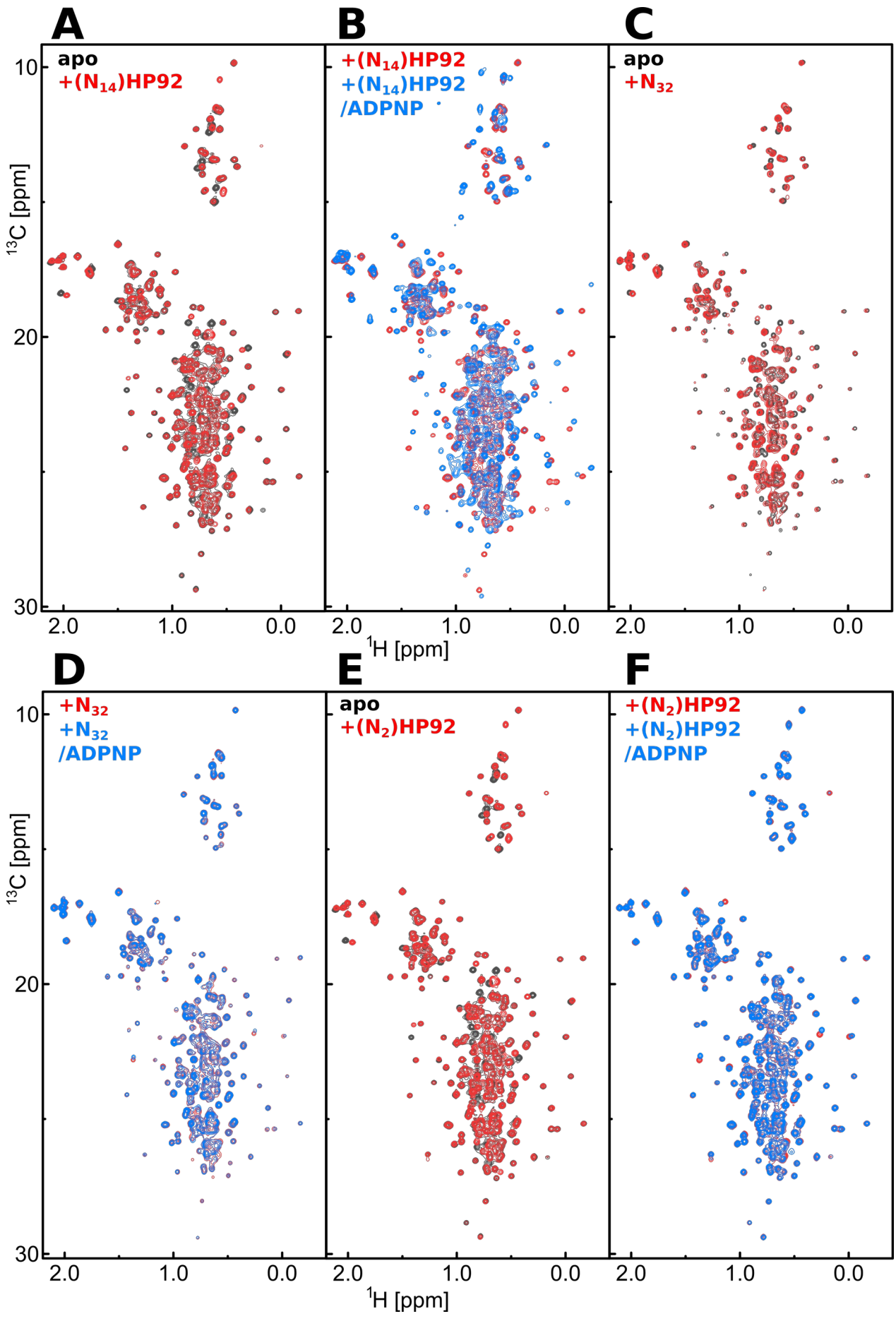
A
apo
+(N14)HP92
B
+(N14)HP92
+(N14)HP92
/ADPNP
C
apo
+N32
D
+N32
+N32
/ADPNP
E
apo
+(N2)HP92
F
+(N2)HP92
+(N2)HP92
/ADPNP
13C [ppm]
1H [ppm]
10
20
30
2.0
1.0
0.0

Fig. S2: Full spectra of RNA and ADPNP titrations to DbpA-wt
Methyl-TROSY spectra of ILMVA-labeled DbpA-wt are shown for the apo state (black), in complex with RNA (red) and in complex with RNA and ADPPNP (blue).
(A, B) Titration of DbpA with (N_{14})HP92 RNA and ADPNP. The closed conformation is formed in the ternary complex (B).
(C, D) Titration of DbpA with N_{32} RNA and ADPNP. No closed conformation is detectable.
(E, F) Titration of DbpA with (N_2)HP92 RNA and ADPNP. No closed conformation is detectable.

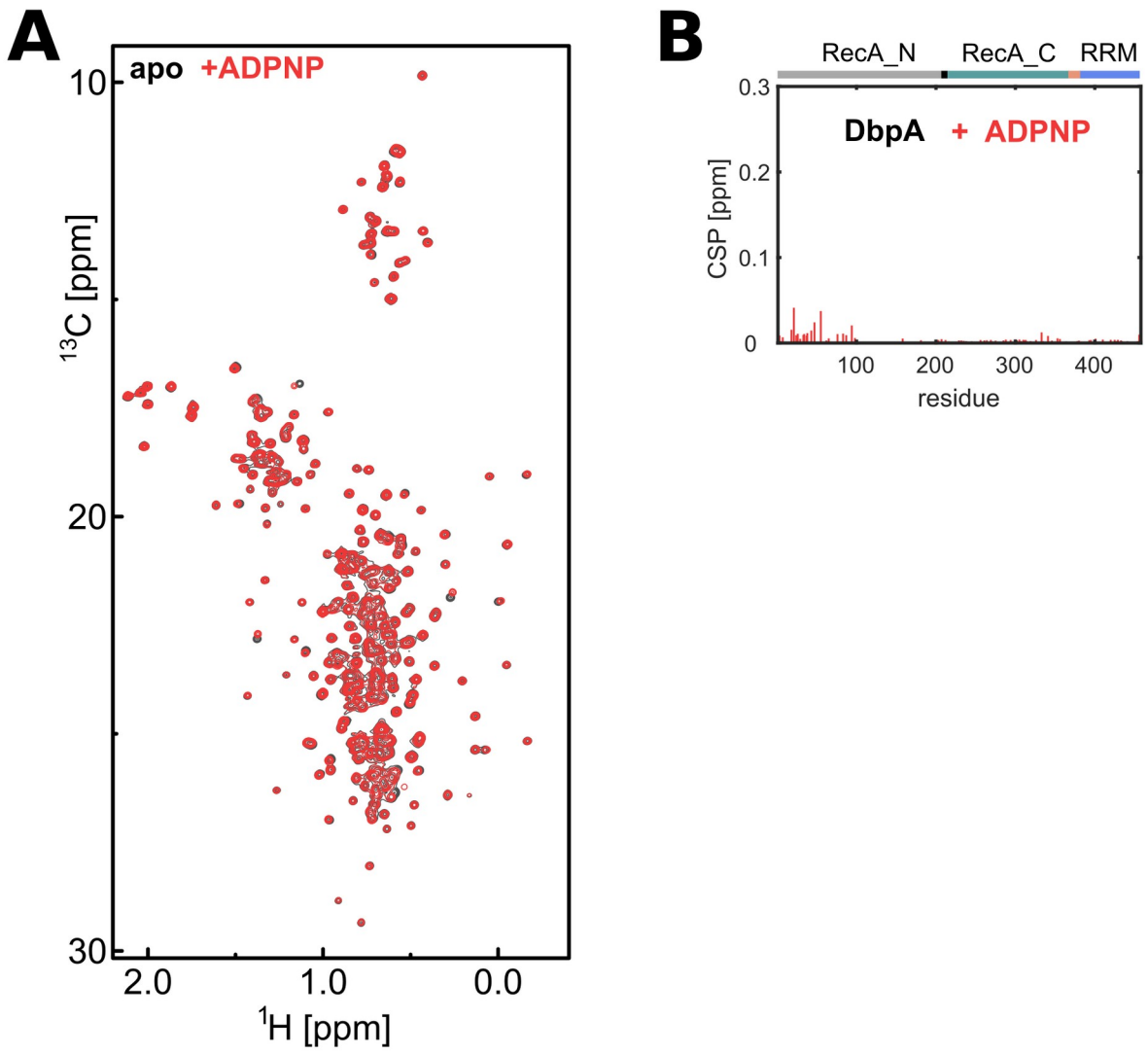

Fig. S3: Binding of ADPNP to DbpA elicits only small CSPs in the RecA_N domain
(A) Methyl-TROSY spectra of ILMVA-labeled DbpA-wt are shown for the apo state (black) and after addition of ADPNP (2 mM).
(B) CSPs elicited by binding of ADPNP to DbpA are plotted against the residue number.

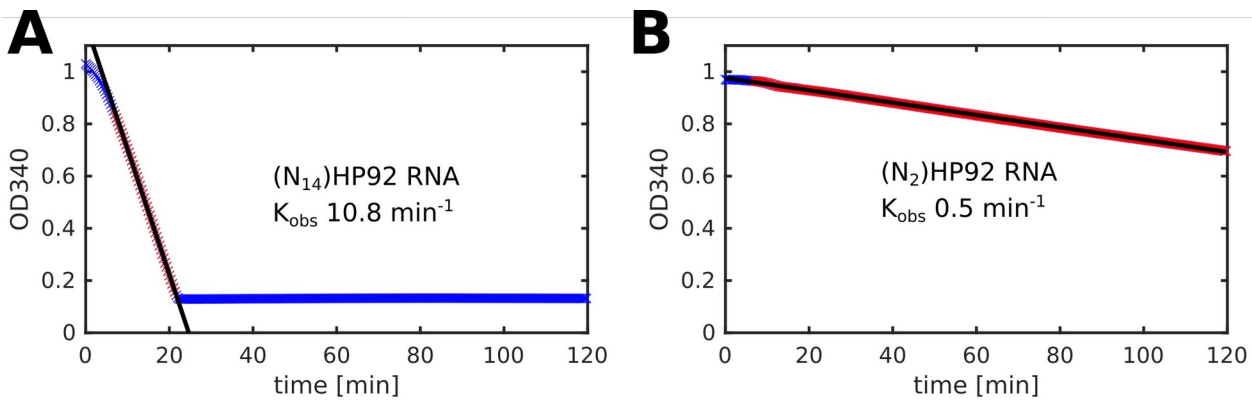

Fig. S4: Exemplary results of ATPase assays for DbpA-wt
Time courses of the coupled pyruvate kinase-lactate dehydrogenase ATPase assay are shown. Oxidation of NADH is followed by absorption measurements at 340 nm (blue and red crosses) every 20 s. Time points in the linear region of the time courses are used for linear regression (shown in red). The fit is shown as a black line. The ATP turnover rates calculated from the slope of the linear regression are given.
(A) ATPase activity of DbpA in complex with the (N_{14})HP92 RNA.
(B) ATPase activity of DbpA in complex with the (N_2)HP92 RNA.

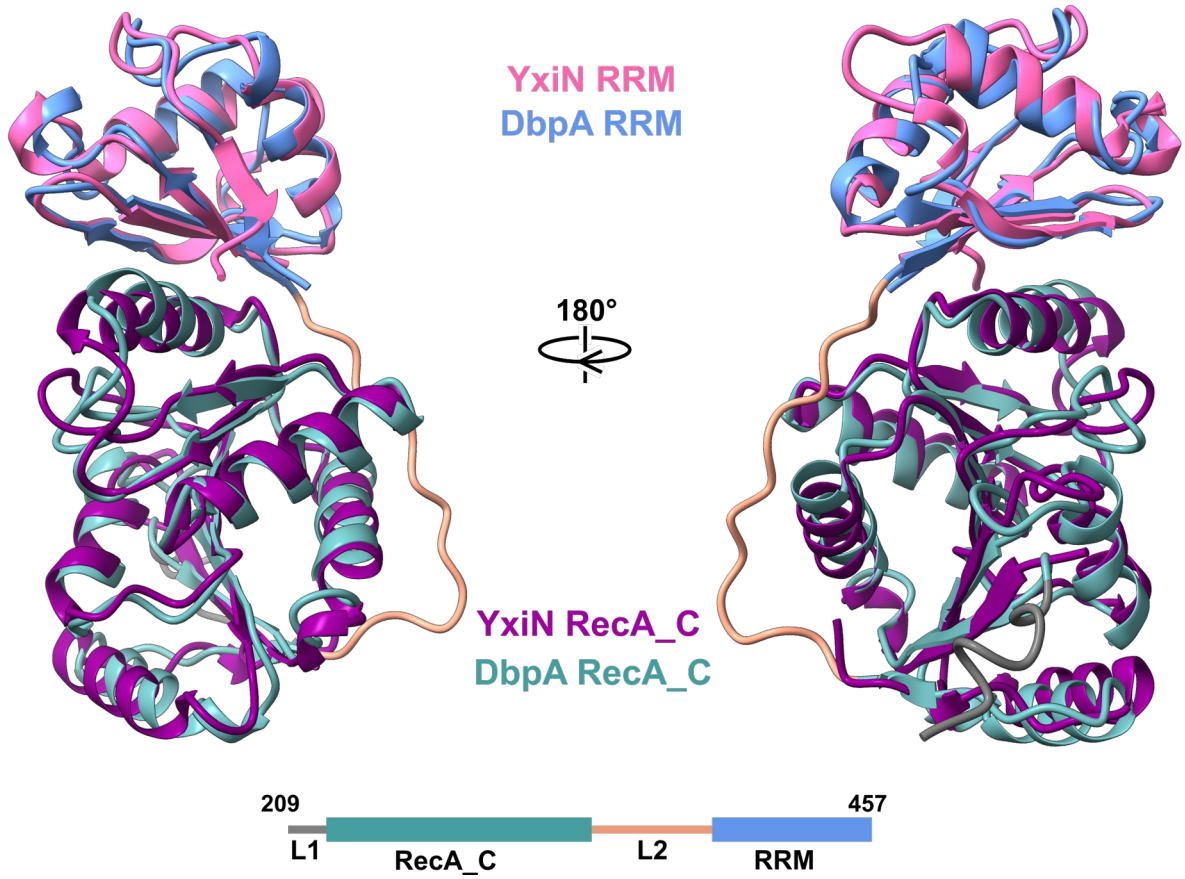

Fig. S5: Comparison between the NMR structure of DbpA that we determined here and the crystal structures of the YxiN RecA_C and RRM domains
The DbpA NMR structure (RecA_C/RRM construct, residues 209-457) with the lowest target function is overlayed with the crystal structures of the isolated YxiN RecA_C domain ((29), PDB ID 2hjv, shown in pink) and the YxiN RRM domain bound to HP92 ((23), PDB ID 3moj, shown in purple). The DbpA construct and color code are shown at the bottom.

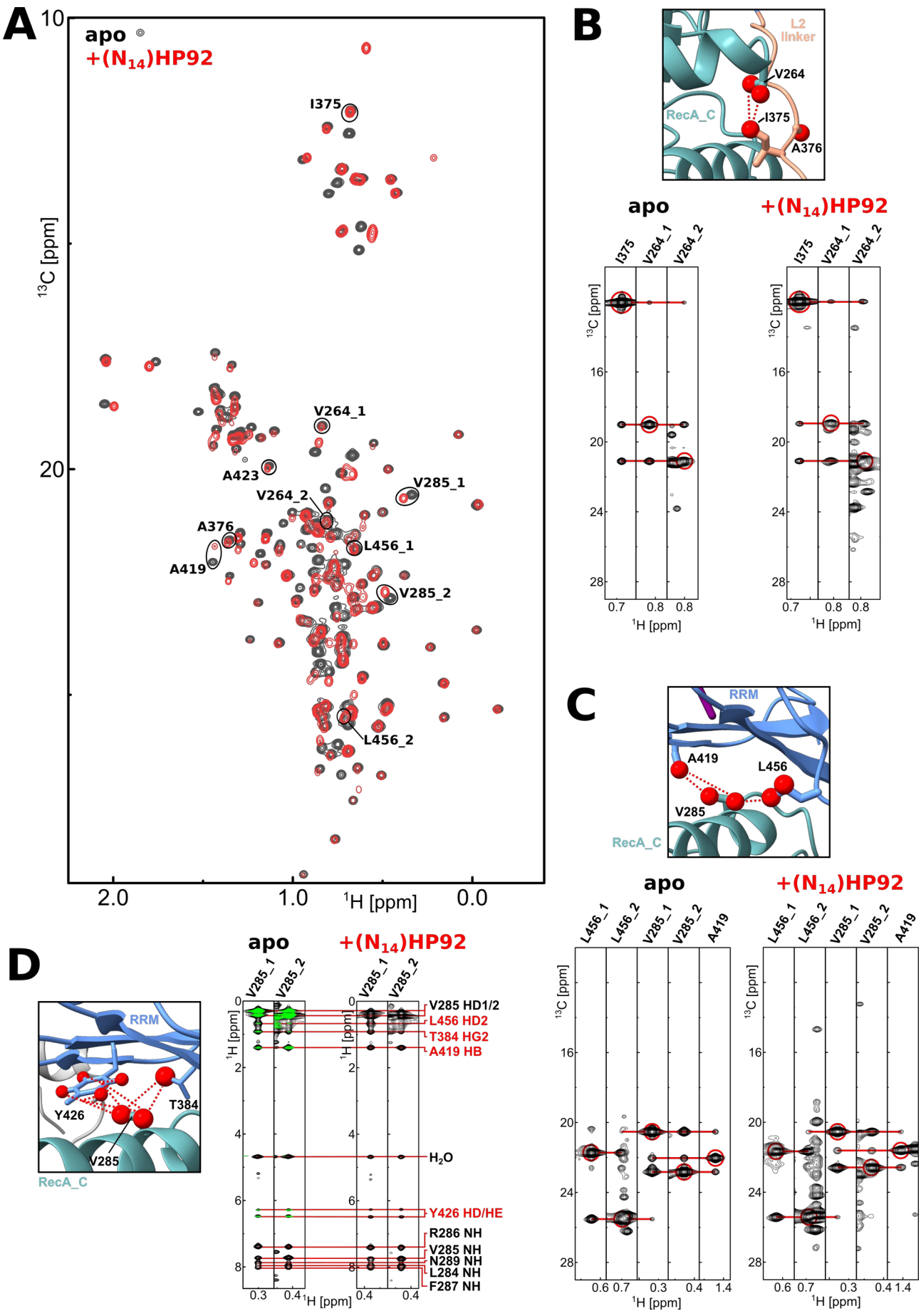
A
apo
+(N14)HP92
I375
V264_1
A423
V264_2
V285_1
A376
L456_1
A419
V285_2
L456_2
13C [ppm]
1H [ppm]
B
L2 linker
V264
RecA_C
I375
A376
apo
+(N14)HP92
I375
V264_1
V264_2
C
RRM
A419
L456
V285
RecA_C
L456_1
L456_2
V285_1
V285_2
A419
D
RRM
T384
Y426
V285
RecA_C
V285 HD1/2
L456 HD2
T384 HG2
A419 HB
H2O
Y426 HD/HE
R286 NH
V285 NH
N289 NH
L284 NH
F287 NH

Fig. S6: CSPs and CCH-NOESY patterns indicate that binding of the (N_{14})HP92 RNA does not change the RecA_C/RRM interdomain orientation.

(A) Overlay of the Methyl-TROSY spectra of the ILMVATY-labeled RecA_C/RRM construct in the apo state (black) and bound to (N_{14})HP92 RNA (red). Residues that mediate the RecA_C/L2 linker (V264, I375, A376) and RecA_C/RRM (V285, A419, L456) contacts are indicated. These residues show only small CSPs indicating the absence of larger conformational changes. As the domain interface between RecA_C and RRM is largely formed by Y426, a change in the interdomain orientation should lead to large CSPs due to the strong influence of ring currents of aromatic residues on chemical shifts. The largest CSP is observed for A419 from the RRM as it is located in the proximity of the RNA binding site.

(B) Comparison of the CCH-NOESY strips for the methyl groups of V264 and I375 in the apo state (ILMVATY-labeled RecA_C/RRM construct) (left) and bound to (N_{14})HP92 RNA (right). Strips are shown along the ^{13}C-NOE dimension. Diagonal peaks are marked by red circles and cross peaks are indicated by red lines. I375 is part of the L2 linker and packs into a hydrophobic pocket of the RecA_C domain in the structure of the RecA_C/RRM construct (top). Very similar NOE cross peaks are observed in both states indicating that the interaction between the L2 linker and the RecA_C domain does not change upon RNA binding.

(C) Comparison of the CCH-NOESY strips for the methyl groups of V285, A419 and L456 in the apo state (ILMVATY-labeled RecA_C/RRM construct) (left) and bound to (N_{14})HP92 RNA (right). A close-up of the interdomain interface is shown on top. The three residues (V285, A419 and L456) are part of the interdomain interface between the RecA_C domain and the RRM. Very similar NOE cross peaks (marked by red lines) are observed in both states indicating that the interdomain orientation does not change upon RNA binding.

(D) Comparison of the HCH-NOESY strips for the methyl groups of V285 in the apo state (ILMVATY-labeled RecA_C/RRM construct) (left) and bound to (N_{14})HP92 RNA (right). NOESY spectra recorded in 95%/5% H_2O/D_2O are shown in black. For the apo state a HCH-NOESY spectrum was also recorded in 100 % D_2O (shown in green). Only NOE crosspeaks to Tyr Hδ/Hε and methyl group resonances are visible in this spectrum. NOE assignments are indicated on the right. Interdomain NOEs between V285 and the RRM are indicated in red. A close-up of the interdomain interface is shown on the left. V285, Y426 and T384 are depicted in stick representation and the observed NOEs between these residues are indicated by dashed red lines. Very similar NOE cross peaks (marked by red lines) are observed in both states indicating that the interdomain orientation does not change upon RNA binding. Note that the methyl group signal of T384 overlaps in the ^{13}C dimension with the signal of V285 and is therefore not visible in the CCH-NOESY strips in panel (C).

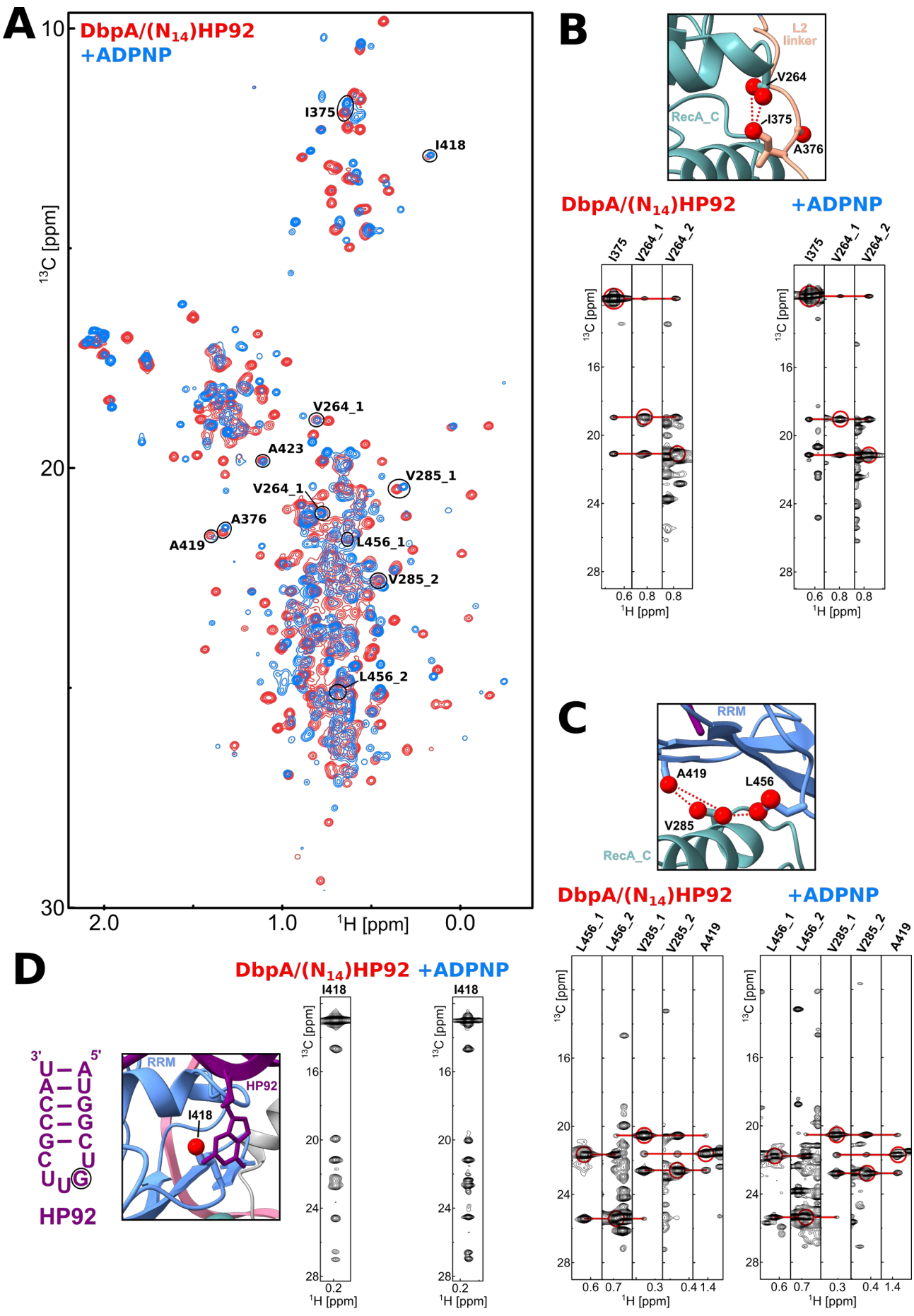
A
DbpA/(N14)HP92
+ADPNP
I375
I418
V264_1
A423
V285_1
V264_1
A376
A419
L456_1
V285_2
L456_2
13C [ppm]
1H [ppm]
B
L2 linker
V264
RecA_C
I375
A376
DbpA/(N14)HP92
+ADPNP
I375
V264_1
V264_2
C
RRM
A419
L456
V285
RecA_C
DbpA/(N14)HP92
+ADPNP
L456_1
L456_2
V285_1
V285_2
A419
D
DbpA/(N14)HP92 +ADPNP
I418
HP92
RRM

Fig. S7: CSPs and CCH-NOESY patterns indicate that the formation of the closed conformation does not change the RecA_C/RRM interdomain orientation.
(A) Overlay of the Methyl-TROSY spectra of the ILMVA-labeled DbpA-wt in complex with (N_{14})HP92 RNA (red) and in the closed state after addition of ADPNP (blue). Residues that mediate the RecA_C/L2 linker (V264, I375, A376) and RecA_C/RRM (V285, A419, L456) and the RRM/HP92 contact (I418) are labeled. These residues show only small CSPs indicating the absence of larger conformational changes. As the interdomain interface between RecA_C and RRM is largely formed by Y426, a change in the interdomain orientation should lead to large CSPs due to the strong influence of ring currents of aromatic residues on chemical shifts. Note that many other signals show large CSPs upon formation of the closed state (see also Fig. 2B of the main text).
(B) Comparison of the CCH-NOESY strips for the methyl groups of V264 and I375 in the (N_{14})HP92 RNA bound state (left) and in the closed state (right). Strips are shown along the ^{13}C-NOE dimension. Diagonal peaks are marked by red circles and cross peaks are indicated by red lines. I375 is part of the L2 linker and packs into a hydrophobic pocket of the RecA_C domain in the structure of the RecA_C/RRM construct (top). Very similar NOE cross peaks are observed in both states indicating that the interaction between the L2 linker and the RecA_C domain does not change upon formation of the closed state.
(C) Comparison of the CCH-NOESY strips for the methyl groups of V285, A419 and L456 in the RNA bound state (left) and in the closed state (right). A close-up of the interdomain interface is shown on top. The three residues are part of the interdomain interface between RecA_C domain and RRM (top).Very similar NOE cross peaks are observed in both states indicating that the interdomain orientation does not change upon formation of the closed state.
(D) Comparison of the CCH-NOESY strips for the Cδ1 methyl group of I418 from the RRM in the (N_{14})HP92 RNA bound state (left) and in the closed state (right). I418 directly interacts with the guanosine in the loop of HP92 (left). Very similar NOE cross peaks are observed in both states indicating that the interaction of the RRM with the loop of HP92 does not change upon formation of the closed state.

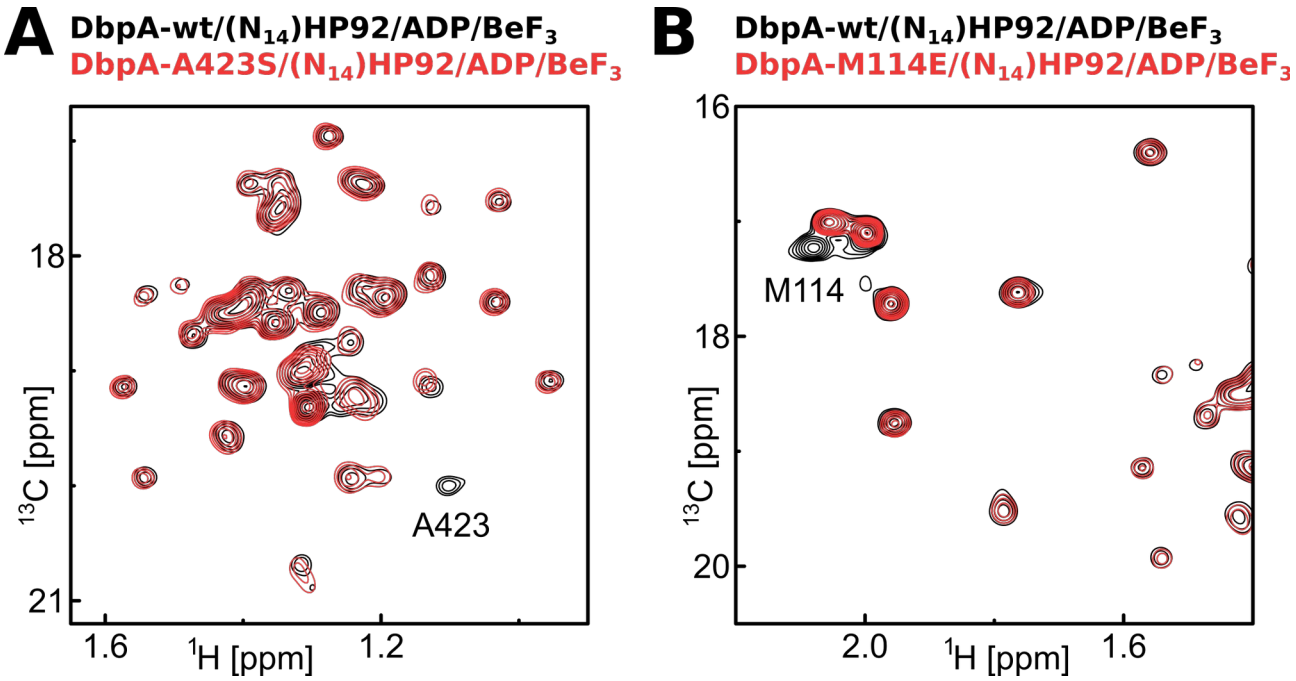

Fig. S8: Assignment of the methyl group signals of A423 and M114 in the closed conformation
The methyl groups were assigned using a mutational approach. Shown are overlays of methyl-TROSY spectra for wt (black) and mutant (red) DbpA in the closed conformation (bound to (N_{14})HP92 RNA and the nonhydrolyzable ATP analog ADP/BeF_3).
(A) The alanine region of the methyl TROSY spectrum is shown. The signal of A423 is assigned based on the comparison between DbpA-wt and the A423S mutant.
(B) The methionine region of the methyl TROSY spectrum is shown. The signal of M114 is assigned based on the comparison between DbpA-wt and the M114E mutant.

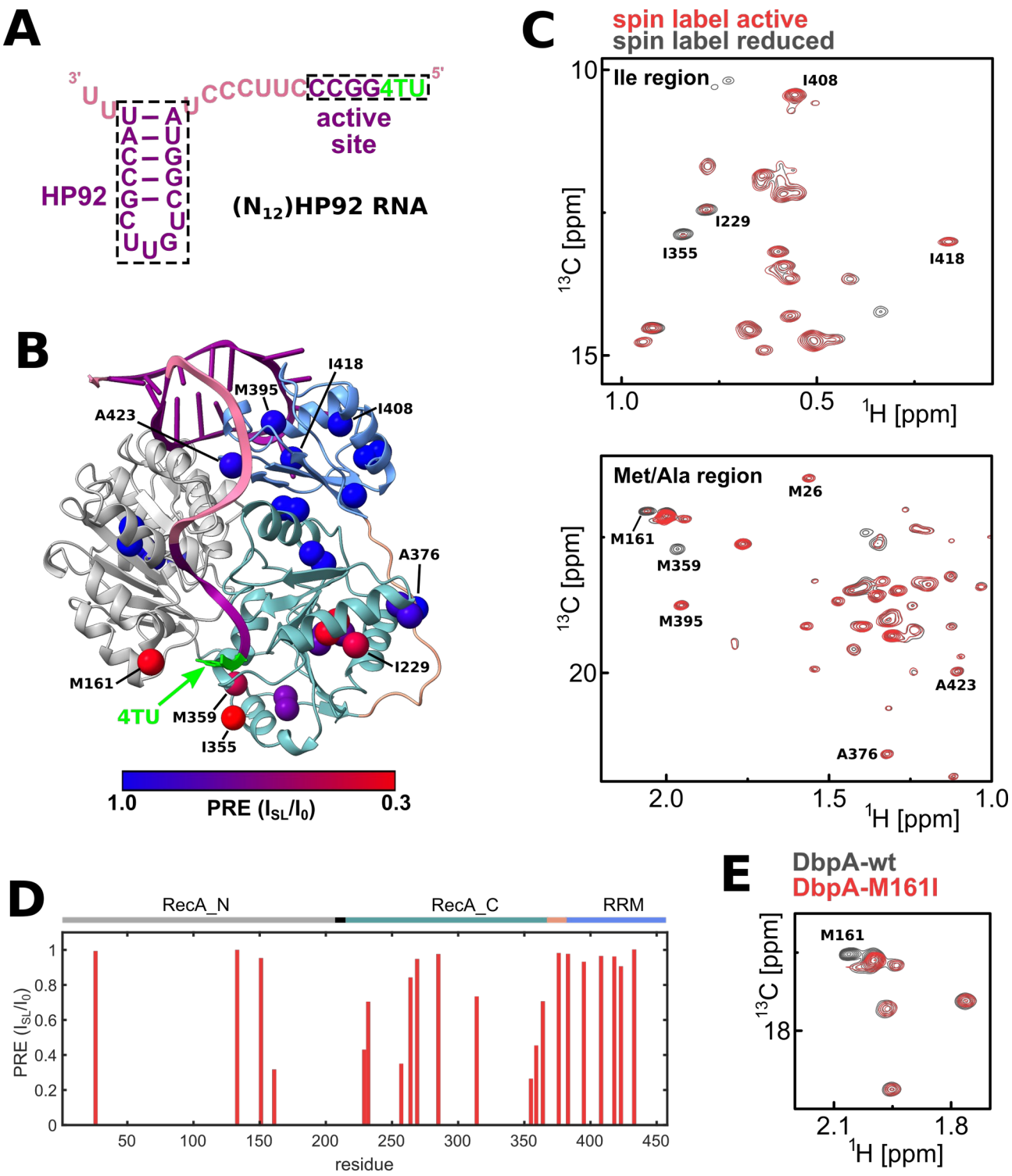

Fig. S9: PRE-experiments with a 5' spin labeled RNA are in agreement with the model of the closed state.

(A) (N_{12})HP92 RNA construct that was used for the PRE-experiments. It contains a 4-Thiouridine (4TU, green) at the 5' end to which the TEMPO spin label was attached. The 5' overhang is shortened by two nt relative to the (N_{14})HP92 RNA to place the spin label closer to the the DbpA core domains. The presence of the spin label leads to a reduction of the intensity of the methyl group NMR signals in its vicinity.

(B) Model of the closed state of DbpA in complex with the (N_{12})HP92 RNA. RRM, RecA_N and RecA_C domains of DbpA are shown in blue, grey and green, respectively. Methyl groups that

could be assigned in the closed state and for which PRE-values could be determined are shown as spheres colored according to the PRE-value (red strong PRE, blue weak PRE). The 4TU nucleotide that carries the spin label is shown in green. Methyl groups that are shown in the spectra in panel C are labeled. The methyl groups that experience strong PREs agree well with the position of the spin label shown in the model.
(C) Methyl-TROSY spectra of ILMVA-labeled DbpA-wt in the closed state in the presence of spin labeled (N_{12})HP92 RNA and ADPNP before (red) and after (black) reduction of the spin label. Close ups of the Ile (top) and Met/Ala (bottom) region of the spectra are shown. Methyl groups that could be assigned in the closed state and for which PRE-values could be determined are labeled.
(D) PRE-values plotted versus the sequence.
(E) Assignment of the methyl group signal of M161 in the closed conformation. M161 is predicted to be in close proximity to the spin label based on our model of the closed state (see (B)) and its methyl group signal could not be assigned in the closed state based on its NOE pattern. It was therefore assigned by mutation to Ile. The Met regions of Methyl-TROSY spectra of DbpA-wt (black) and the DbpA-M161I mutant in the closed conformation bound to (N_{12})HP92 RNA and ADPNP are shown. The signal of M161 is missing in the spectrum of the DbpA-M161I mutant.

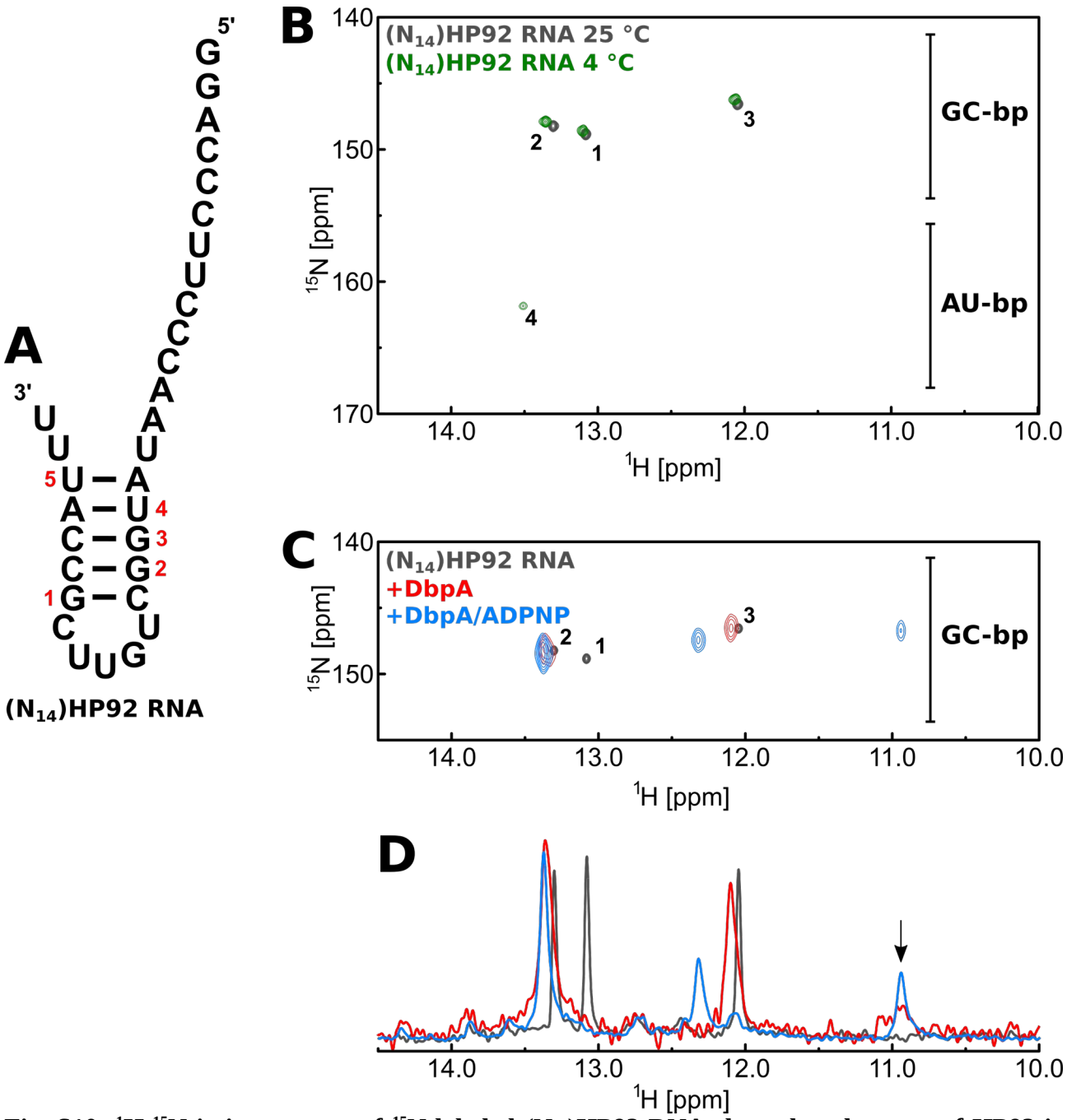

Fig. S10: ^{1}H-^{15}N imino spectra of ^{15}N-labeled (N_{14})HP92 RNA show that the stem of HP92 is still formed in the closed state.

(A) Secondary structure of the (N_{14})HP92 RNA. Imino proton bearing nucleotides of the stem are numbered.

(B) Overlay of the imino region of ^{1}H-^{15}N SOFAST-HMQC spectra of G,U-^{15}N labeled (N_{14})HP92 RNA at 25 °C (black) and 4 °C (green). Imino protons in stable basepairs are protected from exchange with water and are detectable in the ^{1}H-^{15}N SOFAST-HMQC spectra. At 25 °C only the signals of the GC-basepairs of the stem are visible (the imino nitrogen chemical shifts of G and U nucleotides are indicated on the right). The signals are numbered according to (A). At 4 °C the imino proton of U4 is also visible due to slower exchange with water compared to 25 °C.

(C) Overlay of ^{1}H-^{15}N SOFAST-HMQC spectra of the imino region of G,U-^{15}N labeled (N_{14})HP92 in the free state (black), bound to DbpA (red) and in complex with DbpA in the closed state (blue, in the presence of DbpA/ADPNP). Three G imino protons are detectable in the closed state indicating that the stem of HP92 is not disrupted upon formation of the closed state. We tentatively assign the

signal at 10.9 ppm to the G1 imino proton. This basepair is the only basepair that forms a direct contact with the RRM (the sidechain of R396 stacks below the basepair), which would explain the large CSP. A very weak signal is already present at this position in the DbpA bound state (see (D)). The same is observed for several methyl group signals of the RRM that are located in close proximity to the bound RNA and that show weak signal intensities in the RNA bound state, but increased signal intensities in the closed state (see e.g. I418 in figure 2A/B of the main text). We attribute this to residual dynamics of the bound RNA that are quenched upon formation of the closed state.
(D) Overlay of the first points of the indirect dimension of the ^{1}H-^{15}N SOFAST-HMQCs of the G,U-^{15}N labeled (N_{14})HP92 in the free state (black), bound to DbpA (red) and in the closed state (blue). The tentatively assigned G1 imion signal in the closed state is indicated by an arrow. A very weak signal is already present at this position in the spectrum of the DbpA bound state (red).

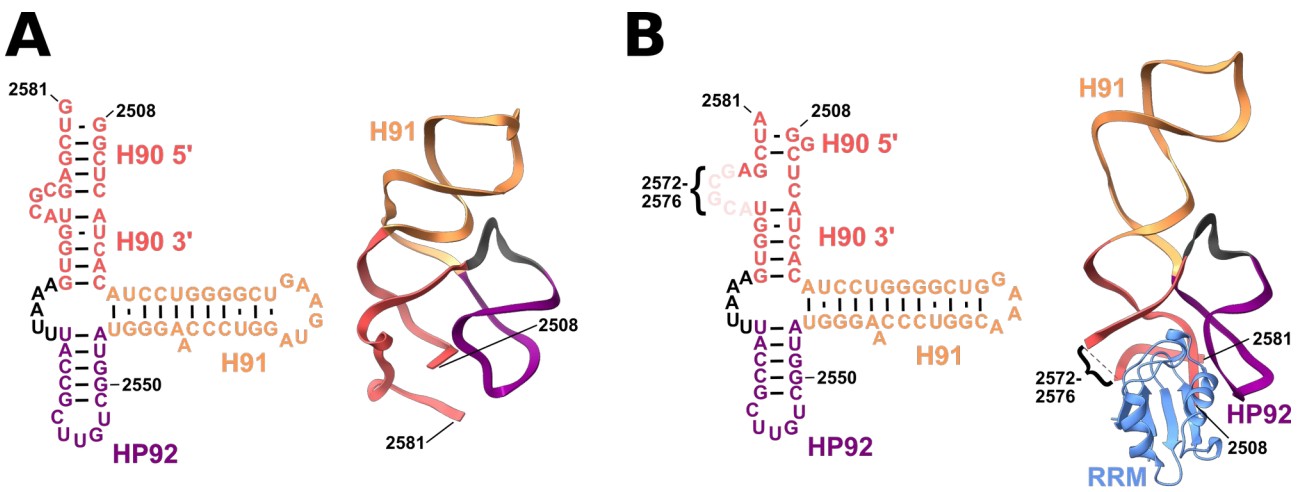

Fig. S11: Helices H90, H91 and HP92 show a similar orientation in the mature ribosome and bound to the YxiN RRM

(A) Secondary (left) and tertiary (right) structure of the 23S rRNA (residues 2508-2581) in the mature 50S subunit (PDB ID 4YBB, (30)). Ribosomal proteins are omitted for clarity. H90, H91 and HP92 are colored red, yellow and violet, respectively.

(B) Secondary (left) and tertiary (right) structure of the 23S rRNA fragments (residues 2508-2581) in complex with the YxiN RRM (PDB ID 3MOJ, (23)). The RRM is shown in light blue. The position of residues 2572-2576 of the 23S rRNA that are not visible in the structure is indicated. Note that the loop sequence of H91 has been changed from GAAGAU in the native 23S rRNA to GGAAAC in the crystallization construct to facilitate crystal formation.

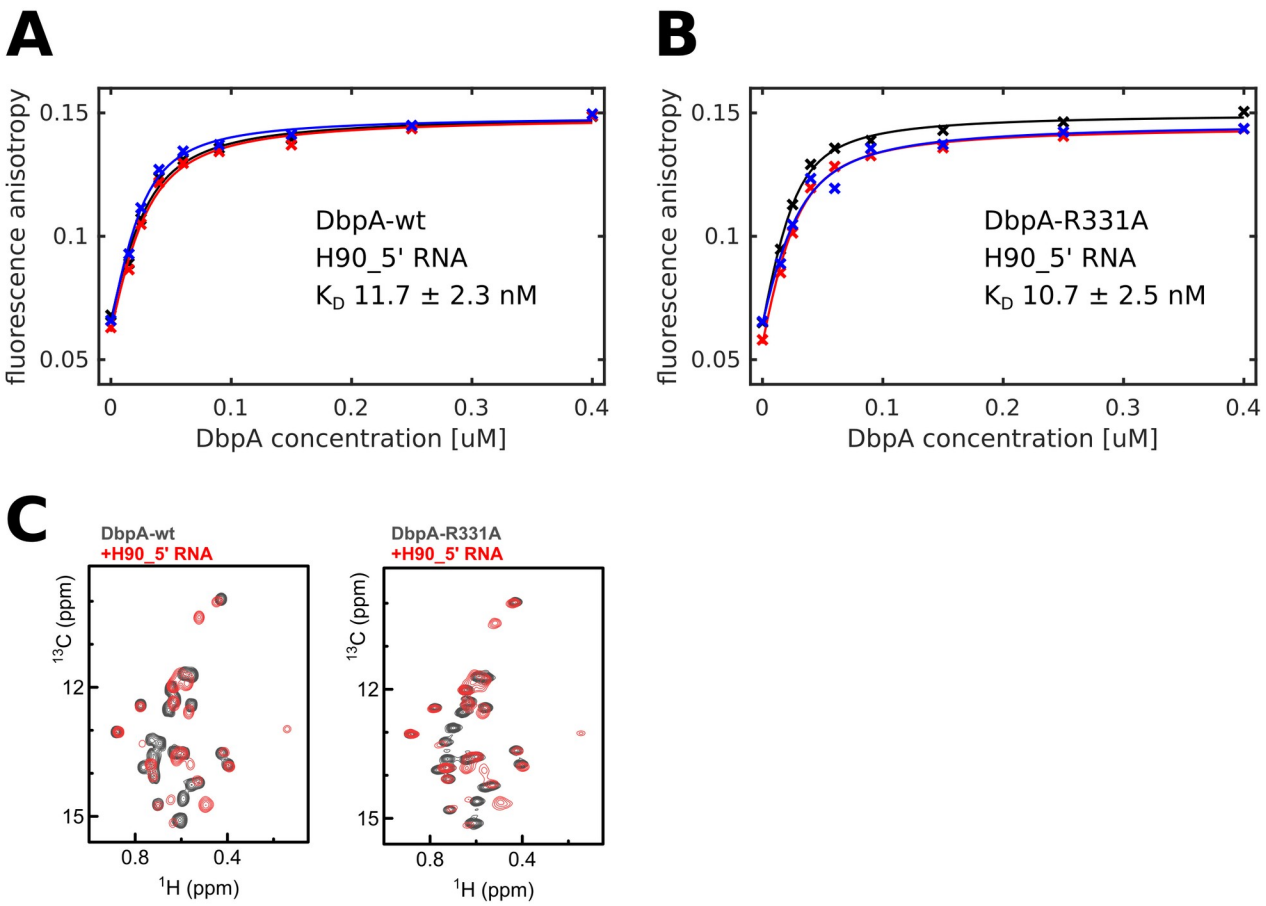

Fig. S12: The R331A mutation does not influence RNA binding
(A,B) Titrations of 3' fluorescein labeled H90_5' RNA with DbpA-wt (A) and DbpA-R331A (B). Binding is followed by fluorescence anisotropy measurements. Titrations were performed in triplicate and are shown in black, red and blue. The dissociation constants were obtained by nonlinear fitting of the data (continues lines). Mean and standard deviation of the three dissociation constants are given.
(C) The Ile-region of methyl-TROSY spectra of ILMVA-labeled DbpA-wt (left) and DbpA-R331A are shown for the apo state (black) and in complex with H90_5' RNA (red). Very similar CSP are observed for wt and mutant DbpA.

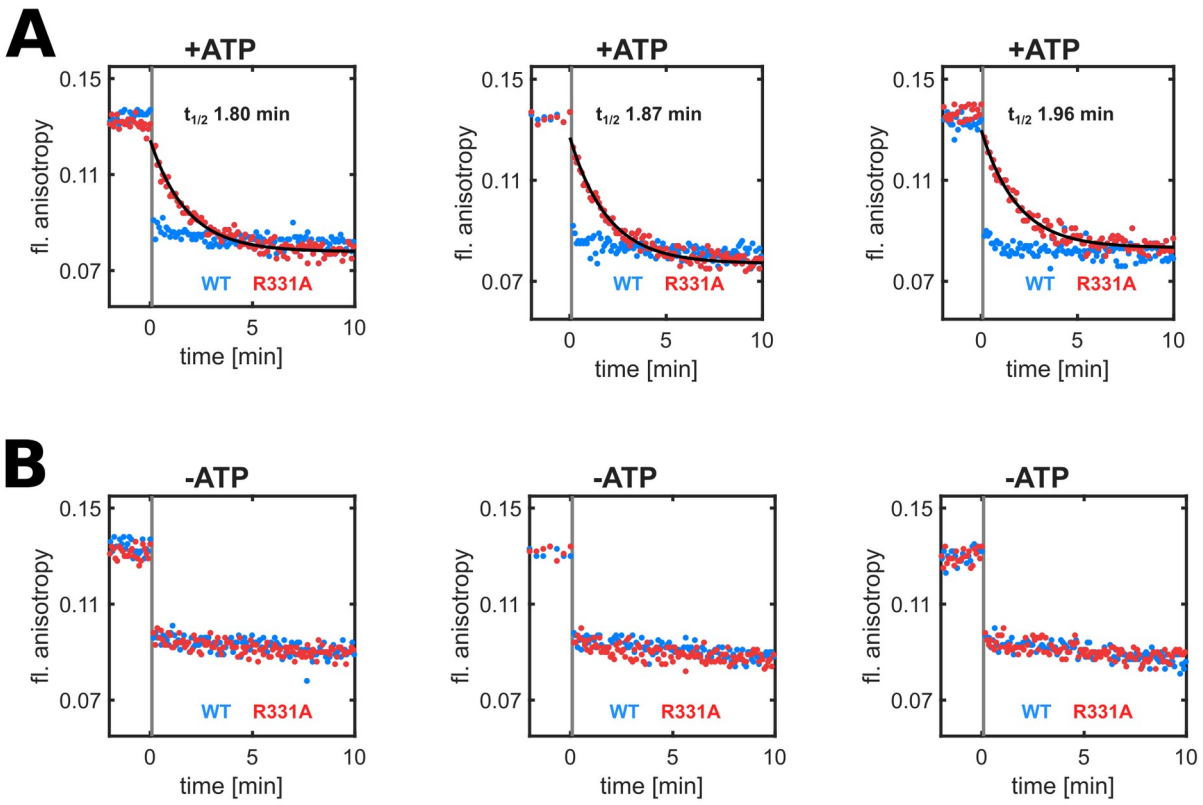

Fig. S13: Replicates of the dissociation rate measurements of the DbpA/H90_5' RNA complex
(A) The three replicates of the fluorescence anisotropy timetraces that follow the dissociation of the complex between DbpA and fluorescently labeled H90_5' RNA. Measurements for DbpA-wt and the R331A mutant are shown in blue and red, respectively. The measurements were conducted in the presence of 2 mM ATP. The halflife of the complex between DbpA-R331A and H90_5' RNA was determined by fitting the data to an exponential decay curve (black line) and is given in the graph. The dead time of the experiment (~10 s) is indicated by a vertical grey bar.
(B) same as (A), but in the absence of ATP.

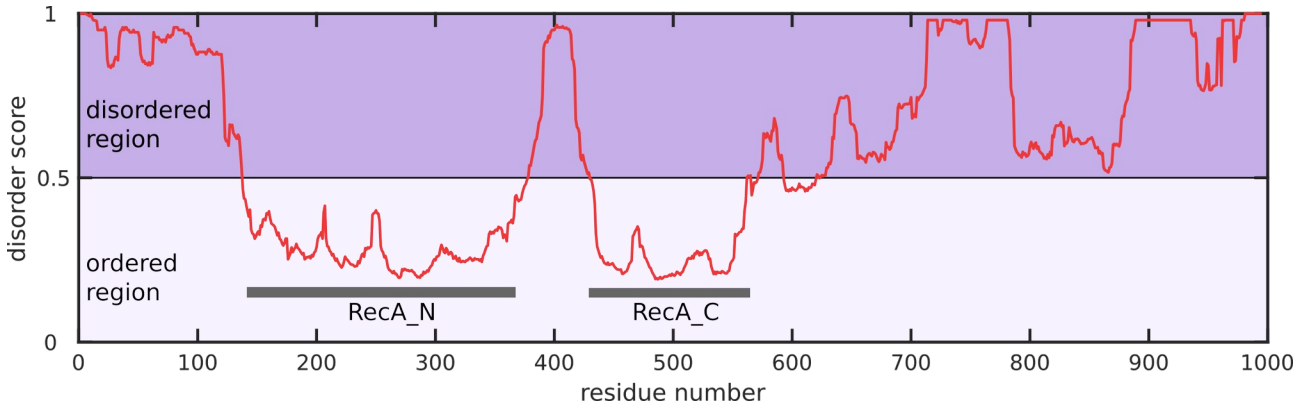

Fig. S14: The flanking regions of *S. cerevisiae* Dbp10 are predicted to be disordered.
Disordered regions of S. cerevisiae Dbp10 were predicted based the amino acid sequence using the metadisordermd2 alogrithm (31). A disorder score > 0.5 indicates unfolded regions. The folded RecA domains are indicated by grey bars.

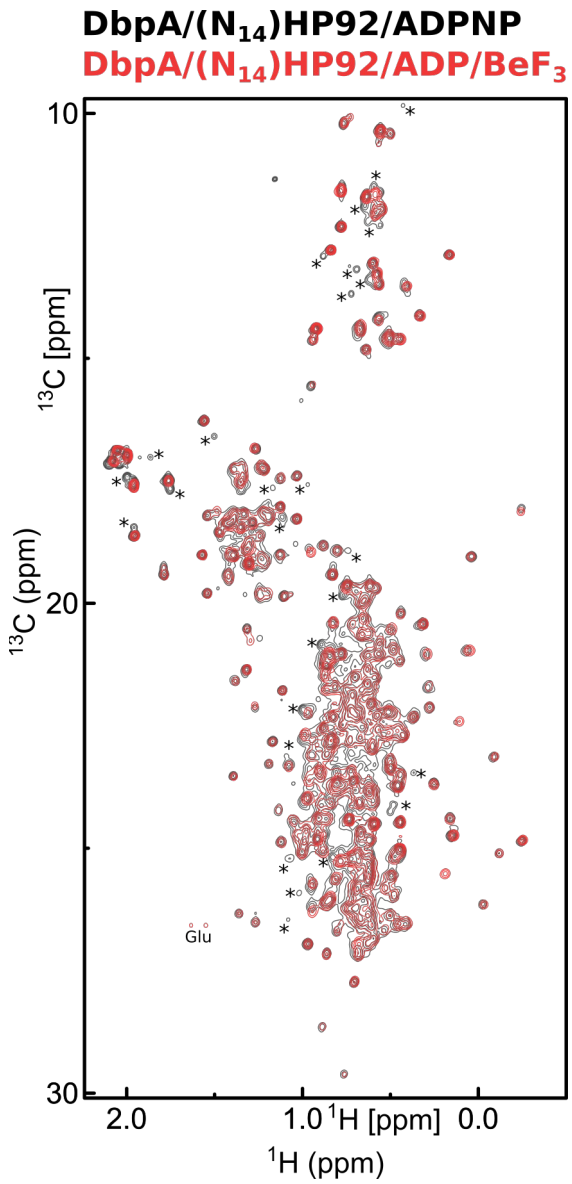

Fig. S15: Spectra of the closed conformation in the presence of ADPNP and ADP/BeF_3 are virtually identical

Methyl-TROSY spectra of ILMVA-labeled DbpA-wt in the presence of (N_{14})HP92 RNA and ADPNP (black) or (N_{14})HP92 RNA and ADP/BeF_3 (red) are shown. The spectra are almost identical indicating that DbpA adopts the same conformation. Weak signals of the open conformation (indicated by asterisks) are visible only in the presence of ADPNP. In the presence of ADP/BeF_3 the population of the open conformation is below the detection limit. The natural abundance signal of a glutamate side chain methylene group is labeled with Glu. The sample in the presence of ADP/BeF_3 was used for the NOE measurements shown in Fig. 4 of the main text and 25 mM Arg/Glu was added to the buffer to increase the long term stability of the sample.

Table S1: Structure statistics of the DbpA NMR structure (residues 209-457).

Restraint statistics	
Total NOE distance restraints	3305
intra residue |i-j|=0	190 (5.7 %)
sequential |i-j|=1	533 (16.1 %)
medium range 1<|i-j|<5	746 (22.6 %)
long range |i-j|≥5	1836 (55.6 %)
interdomain (between res. 214-374 and res. 375-457)	88 (2.7 %)
NOE distance restraints per residue	13.2
Hydrogen bond restraints	58
Dihedral restraints (TALOS-N)	414
Target function	10.7 ± 1.4
Distance restraint violations	
Number of violations > 0.1 Å	76 ± 13
RMS (Å)	0.015 ± 0.001
Maximum violation (Å)	0.46 ± 0.08
Dihedral angle restraints violation	
Number of violations > 5 °	3 ± 1
RMS (°)	1.0 ± 0.1
Maxiumum violation (°)	9.0 ± 2.6
Structural statistics	
Ramachandran plot statistics [%]	
Residues in most favored regions	85.3
Residues in additionally allowed regions	14.3
Residues in generously allowed regions	0.5
Residues in disallowed regions	0
RMSD values (ordered residues, 214-457)	
backbone (Å)	0.6 ± 0.1
heavy atoms (Å)	1.1 ± 0.1

Table S2: DbpA constructs used in this study.

protein	residues	mutation	internal reference
DbpA wt	1-457	-	#1705
DbpA RecA_C/RRM	209-457	-	#1763
DbpA-R331A	1-457	R331A	#1884
DbpA-R96A	1-457	R96A	#1995
DbpA-M114E	1-457	M114E	#1999
DbpA-K102A	1-457	K102A	#2022
DbpA-R92A	1-457	R92A	#2058
DbpA-M161I	1-457	M161I	#1988
DbpA-A423S	1-457	A423S	#2068

Table S3: RNA constructs used in this study.

RNA	sequence	internal reference
N_{32}	5'GGCAAAUGAGGUCCCAAGCGUACUGUUCCGUC3'	#139
(N_{14})HP92	5'GGACCCUUCCCAAUAUGGCUGUUCGCCAUUU3'	#42
(N_{2})HP92	5'GGAUGGCUGUUCGCCAUUU3'	#144
(N_{12})HP92	5'(4TU)GACCCUUCCCUAUGGCUGUUCGCCAUUU3'	
N_{9}	5'Fl-UUGGGACCU3' / 5'UUGGGACCU3'	
$N_{9'}$	5'Fl-GGGAAGGGU3' / 5'GGGAAGGGU3'	
S (HP92 stem)	5'GGGCUGUUCGCCC3'	#128
H + 2nt 5'	5'GGAUGGCUGUUCGCCAUUU3'	#144
H + 4nt 5'	5'GGACAUGGCUGUUCGCCAUUU3'	#134
H + 9nt 5'	5'GGACAUAUGGCUGUUCGCCAUUU3'	#135
H + 8nt 5'	5'GGAACACUAUGGCUGUUCGCCAUUU3'	#146
H + 10nt 5'	5'GGACUACACUAUGGCUGUUCGCCAUUU3'	#143
H + 12nt 5'	5'GGAACCAAGGCCAUGGCUGUUCGCCAUUU3'	#122
H90_5'	5'GGCACCUCGAUGUCGGCUCAUCACAUCCUGGGGCUGAAGUAGGUCCCAAG GGUAUGGCUGUUCGCCAUUUAAAGUGGUACGCGAGCUGGG3'	#91/109
H90_3'	5'GGCUCAUCACAUCCUGGGGCUGAAGUAGGUCCCAAGGGUAUGGCUGUUCG CCAUUUAAAGUGGUACGCGAGCUGGGUUUAGAACGUCGUGAGACAGUUC3'	#93/95

Fl indicates a 5' fluorescein label, (4TU) indicates a 4-Thiouridine residue. N_9 and $N_{9'}$ were used in unlabeled and 5' fluorescein labeled form for helicase assays.

SI References

1. R. J. Lichtenecker, K. Weinhäupl, W. Schmid, R. Konrat, α-Ketoacids as precursors for phenylalanine and tyrosine labelling in cell-based protein overexpression. *J. Biomol. NMR* **57**, 327–331 (2013).

2. R. M. Rasia, B. Brutscher, M. J. Plevin, Selective isotopic unlabeling of proteins using metabolic precursors: application to NMR assignment of intrinsically disordered proteins. *Chembiochem* **13**, 732–739 (2012).

3. J. P. Wurm, Assignment of the Ile, Leu, Val, Met and Ala methyl group resonances of the DEAD-box RNA helicase DbpA from E. coli. *Biomol NMR Assign* (2020) https:/doi.org/10.1007/s12104-020-09994-z.

4. D. Neri, T. Szyperski, G. Otting, H. Senn, K. Wüthrich, Stereospecific nuclear magnetic resonance assignments of the methyl groups of valine and leucine in the DNA-binding domain of the 434 repressor by biosynthetically directed fractional 13C labeling. *Biochemistry* **28**, 7510–7516 (1989).

5. P. Güntert, L. Buchner, Combined automated NOE assignment and structure calculation with CYANA. *J. Biomol. NMR* **62**, 453–471 (2015).

6. P. Rossi, Y. Xia, N. Khanra, G. Veglia, C. G. Kalodimos, 15N and 13C- SOFAST-HMQC editing enhances 3D-NOESY sensitivity in highly deuterated, selectively [1H,13C]-labeled proteins. *J. Biomol. NMR* **66**, 259–271 (2016).

7. Y. Xu, Y. Zheng, J.-S. Fan, D. Yang, A new strategy for structure determination of large proteins in solution without deuteration. *Nat. Methods* **3**, 931–937 (2006).

8. W. Lee, M. Tonelli, J. L. Markley, NMRFAM-SPARKY: enhanced software for biomolecular NMR spectroscopy. *Bioinformatics* **31**, 1325–1327 (2015).

9. Y. Shen, A. Bax, Protein backbone and sidechain torsion angles predicted from NMR chemical shifts using artificial neural networks. *J. Biomol. NMR* **56**, 227–241 (2013).

10. D. Gottstein, D. K. Kirchner, P. Güntert, Simultaneous single-structure and bundle representation of protein NMR structures in torsion angle space. *J Biomol NMR* **52**, 351–364 (2012).

11. E. F. Pettersen, *et al.*, UCSF ChimeraX: Structure visualization for researchers, educators, and developers. *Protein Sci* **30**, 70–82 (2021).

12. N.-A. Lakomek, J. Ying, A. Bax, Measurement of ^{15}N relaxation rates in perdeuterated proteins by TROSY-based methods. *J Biomol NMR* **53**, 209–221 (2012).

13. M. P. Williamson, Using chemical shift perturbation to characterise ligand binding. *Progress in Nuclear Magnetic Resonance Spectroscopy* **73**, 1–16 (2013).

14. F. Delaglio, *et al.*, NMRPipe: A multidimensional spectral processing system based on UNIX pipes. *Journal of Biomolecular NMR* **6** (1995).

15. R. Keller, *The computer aided resonance assignment tutorial* (Cantina Verl., 2004).

16. C. A. Tsu, O. C. Uhlenbeck, Kinetic analysis of the RNA-dependent adenosinetriphosphatase activity of DbpA, an Escherichia coli DEAD protein specific for 23S ribosomal RNA. *Biochemistry* **37**, 16989–16996 (1998).

17. K. Kiianitsa, J. A. Solinger, W.-D. Heyer, NADH-coupled microplate photometric assay for kinetic studies of ATP-hydrolyzing enzymes with low and high specific activities. *Anal Biochem* **321**, 266–271 (2003).

18. J. Guillerez, P. J. Lopez, F. Proux, H. Launay, M. Dreyfus, A mutation in T7 RNA polymerase that facilitates promoter clearance. *Proc. Natl. Acad. Sci. U.S.A.* **102**, 5958–5963 (2005).

19. J. F. Milligan, D. R. Groebe, G. W. Witherell, O. C. Uhlenbeck, Oligoribonucleotide synthesis using T7 RNA polymerase and synthetic DNA templates. *Nucleic Acids Res.* **15**, 8783–8798 (1987).

20. E. F. Pettersen, *et al.*, UCSF Chimera--a visualization system for exploratory research and analysis. *J Comput Chem* **25**, 1605–1612 (2004).

21. T. Sengoku, O. Nureki, A. Nakamura, S. Kobayashi, S. Yokoyama, Structural Basis for RNA Unwinding by the DEAD-Box Protein Drosophila Vasa. *Cell* **125**, 287–300 (2006).

22. A. Waterhouse, *et al.*, SWISS-MODEL: homology modelling of protein structures and complexes. *Nucleic Acids Research* **46**, W296–W303 (2018).

23. J. W. Hardin, Y. X. Hu, D. B. McKay, Structure of the RNA binding domain of a DEAD-box helicase bound to its ribosomal RNA target reveals a novel mode of recognition by an RNA recognition motif. *J. Mol. Biol.* **402**, 412–427 (2010).

24. N. R. Zearfoss, S. P. Ryder, End-labeling oligonucleotides with chemical tags after synthesis. *Methods Mol Biol* **941**, 181–193 (2012).

25. B. E. Suzek, *et al.*, UniRef clusters: a comprehensive and scalable alternative for improving sequence similarity searches. *Bioinformatics* **31**, 926–932 (2015).

26. F. Sievers, D. G. Higgins, Clustal Omega for making accurate alignments of many protein sequences. *Protein Sci* **27**, 135–145 (2018).

27. G. E. Crooks, G. Hon, J.-M. Chandonia, S. E. Brenner, WebLogo: a sequence logo generator. *Genome Res* **14**, 1188–1190 (2004).

28. K. J. Polach, O. C. Uhlenbeck, Cooperative binding of ATP and RNA substrates to the DEAD/H protein DbpA. *Biochemistry* **41**, 3693–3702 (2002).

29. J. M. Caruthers, Y. Hu, D. B. McKay, Structure of the second domain of the Bacillus subtilis DEAD-box RNA helicase YxiN. *Acta Crystallogr. Sect. F Struct. Biol. Cryst. Commun.* **62**, 1191–1195 (2006).

30. J. Noeske, *et al.*, High-resolution structure of the Escherichia coli ribosome. *Nat Struct Mol Biol* **22**, 336–341 (2015).

31. L. P. Kozlowski, J. M. Bujnicki, MetaDisorder: a meta-server for the prediction of intrinsic disorder in proteins. *BMC Bioinformatics* **13**, 111 (2012).